Controlling the CO_2 Reduction Reaction through Dual-Atom Catalysts Embedded in Expanded Porphyrins: A DFT Study

Gavin A. McCarver,* Taner Yildirim, and Wei Zhou

National Institute of Standards and Technology, Center for Neutron Research, Gaithersburg, Maryland 20899-6102, United States

E-mail: gavin.mccarver@nist.gov

Abstract

In the pursuit of innovative molecular catalysts for the electrocatalytic reduction of CO_2, we employed computational methodologies to investigate six Cu-based expanded porphyrin dual-atom catalysts (DACs). Our study revealed both large and small variations among the different DACs. Despite metal center substitutions, the highly delocalized nature of the π orbitals in the expanded porphyrin complexes led to minimal differences between the frontier orbitals. Conversely, pronounced differences emerged during hydrogen reduction. Notably, the formation of H_2 exhibited low limiting potentials ranging from 0.13 to 0.43 eV, attributable to the ligand-centered activity of the expanded porphyrin. Similar limiting potentials (< 0.31 eV) for CO_2 reduction indicate competition between the two reduction processes. This can be attributed to the emergence of highly favorable bridging μ_2 intermediates, exemplified by *OCHO and *OH. The preference for these intermediates is expected to lead to the formation of only $2e^-$ and $4e^-$ products, namely H_2, HCOOH and H_2CO. Specifically, CuFe and CuMn DACs are poised to favor CO_2 reduction to produce HCOOH and H_2CO, while CuCo, CuCu, and CuZn DACs are anticipated to favor the production of H_2.

Introduction

The continual burning of fossil fuels in the modern world is expected to cause significant changes in climate caused by increased levels of anthropogenic carbon dioxide (CO_2) in the atmosphere.[1] Recent atmospheric measurements have detected CO_2 levels reaching 421 parts per million (ppm), surpassing pre-industrial levels by over 50%, with projections indicating further increases unless effective mitigation strategies are implemented. To address this environmental challenge and meet current climate objectives, researchers have intensified their efforts in developing and refining carbon capture, utilization, and sequestration (CCUS) technologies.[2,3] These multifaceted approaches encompass the capture of CO_2 from both atmospheric[4] and industrial sources,[5] the conversion of CO_2 into high-value feedstock materials and fuels,[6] and the long-term sequestration of CO_2 in mineral deposits.[7]

Current techniques for the conversion and utilization of CO_2 encompass diverse methodologies, including electrocatalytic reduction,[8] thermal activation,[9–11] and photochemical conversion.[12] The outcome of these techniques is heavily dependent on the physical properties and electronic structures of the chosen catalysts.[13] Of particular interest are single-atom catalysts (SAC), where the active metal center and support play a pivotal role in reducing CO_2.[14–16] Research has demonstrated substantial variations in product formation when different transition metals (TM) are employed as SACs. Abdinejad *et al.*[17] and Call *et al.*[18] utilized tetraphenylporphyrin-based molecular electrocatalysts to reduce CO_2 using different transition metal active sites. Abdinejad *et al.* utilized a Mn-based porphyrin catalyst, which promoted the conversion of CO_2 to acetate, while Call *et al.* utilized a Co-based analogue that exhibited a high degree of selectivity for CO_2 reduction to CO. This significant disparity in product formation stems from the distinct electronic structures imparted by the metal active sites.

In the pursuit of further refining the CO_2 reduction reaction (CO_2RR), researchers have

designed materials with secondary active sites, enabling subtle alterations in chemistry. These innovative dual-atom catalysts (DAC) have emerged as invaluable tools for elucidating the intrinsic (electronic) structure-function relationships inherent in catalytic systems.[19–23] Moreover, physical characteristics, such as the intermetallic distance between active sites, offer additional facets to optimize and fine-tune CO_2RR. An illustrative example of a DAC with intrinsic metal-metal interactions lies in a recent study by Ding *et al.*,[24] where Fe-Mo DAC sites were designed close together to lower the energy barrier associated with the initial CO_2 reduction. This strategic adjustment led to a more favorable and selective production of CO. Conversely, in a different approach, Qiu *et al.*[25] designed a metal-organic framework (MOF) electrocatalyst with minimal metal-metal interactions. The material featured different Cu active sites far from each other that facilitated the selective reduction of CO_2 to ethylene (C_2H_4). The sites worked synergistically with one reducing CO_2 to CO while the other reduced that CO molecule selectively to ethylene. The strategic utilization of two metal centers, such as those explored by Qiu *et al.* and Ding *et al.*, not only deepens our comprehension of structure-function relations in CO_2 reduction but also opens up new prospects for enhancing electrocatalytic performance in sustainable energy conversion and utilization processes.

In this study, we investigate the use of Cu-based DAC systems incorporated within an expanded porphyrin (EP) framework[26] as CO_2 reduction catalysts. Our primary objective is to gain insight into the influence of the secondary metal on CORR, specifically as it relates to the preference towards either HCOOH or H_2CO production. In addition to this, we examine the hydrogen evolution reaction (HER) and the level of competitiveness expected between HER and CO_2RR on the EP-based DAC catalysts. Central to this exploration is the examination of the non-innocent behavior exhibited by the porphyrinic nitrogen atoms, which serve as the sites for hydrogen reduction to H_2. We then present an extensive analysis of the CO_2 reduction process, elucidating the effects of the secondary metal within the DAC.

By scrutinizing this critical aspect, we aim to better understand the underlying mechanisms that govern the reduction mechanisms on the DAC systems. A better understanding of the Cu-based, EP-incorporated DAC may lead to improvement on current DAC systems for CO_2 reduction.

Computational Methods

To investigate the reduction of CO_2 on the Cu-based, DAC-incorporated EP, we utilized a model system derived from the bis[(μ-chloro) copper(II)] amethryin molecular complex synthesized by Weghorn *et al.*.[26] These systems are denoted as CuX, where X represents the secondary TM. To simplify the EP structure, the -CH_3 and -CH_2CH_3 functional groups were replaced with hydrogen atoms (Scheme 1). Additionally, the Cl^- groups were removed, assuming two initial reductions yielding two Cl^- anions and the charge-neutral EP complex, following previous examples in the literature.[27,28] While these simplifications may impact the final results, we expect the changes to be systematic and consistent across all systems. To understand how the choice of secondary metal affects CO_2RR, one of the Cu atoms in the EP was substituted with another 3d transition metal, including Mn, Fe, Co, Ni, and Zn. For each metal-substituted EP, we explored low-, intermediate-, and high-spin states when applicable to determine the most energetically favorable spin state (Table S1).

Our computational approach follows previous work[29–31] and utilizes the B3LYP density functional[32,33] as implemented in the ORCA 5.0.3 software package.[34] Tight convergence criteria are employed for both the SCF iterations and geometry optimization cycles. Dispersion corrections were accounted for using the D3 method[35] with the Becke-Johnson damping factor (D3BJ).[36] Unrestricted Kohn-Sham wave functions were assumed for each calculation, employing the resolution of identity chain-of-spheres (RIJCOSX)[37] method with the def2/J auxiliary basis set.[38] The def2-TZVP basis set was used for the 3d transition metals, the first

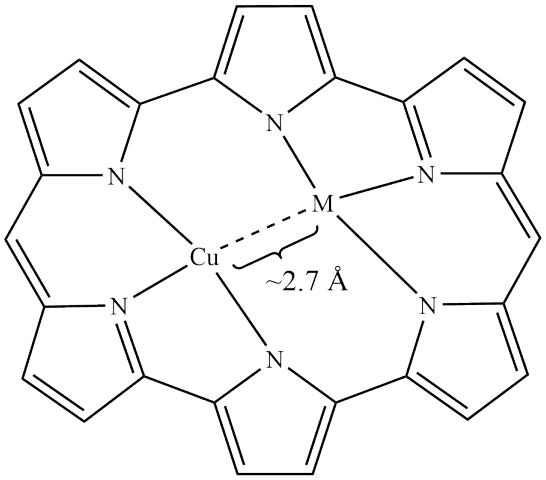

M = Mn, Fe, Co, Ni, Cu, Zn

Scheme 1: Model complex for the Cu-based, DAC-incorporated EP.

coordination sphere around each metal, and the adsorbate molecules, while the def2-SV(P) basis set was used for all other atoms. Analytical frequency calculations were performed to ensure that each structure represents a local minima on the potential energy surface. The conductor-like polarizable continuum model (C-PCM) was applied to approximate the implicit solvation environment around the expanded porphyrin.[39] We used H_2O as our chosen solvent. Charge model 5 (CM5) partial atomic charges[40] were calculated using the Multiwfn program.[41]

To calculate the free energy (G) of each reactant, intermediate, and product, we employed a composite scheme (Eq. 1). This scheme includes the total electronic energy (E), corrections for the inner energy composed of the zero-point energy and thermal effects (I), enthalpic (H) and entropic (S) corrections at T = 298.15 K, and corrections due to the implicit solvation model ($\Delta E_{C\text{-}PCM}$). The optimizations and frequency calculations were performed in the gas-phase which were then followed by a single-point calculation with the solvation model using the gas-phase optimized geometry in order to calculate the $\Delta E_{C\text{-}PCM}$ term of Eq. 1. For electrochemical steps involving a reduction via a proton-coupled electron transfer (PCET)

mechanism, we introduced an additional energy term, eU, to simulate the effect of an applied potential (U) for each elementary step.[42,43] The limiting potential (or overpotential, U_L) for each product is determined based on the largest free energy difference between elementary steps (ΔG_{max}). The reactants for each reduction step consist of the expanded porphyrin, CO_2, and H^+/e^- pairs. The energy of a single H^+/e^- pair is referenced to one-half the energy of H_2 at the given level of theory according to the computational hydrogen electrode (CHE).[13,44]

$$G = E + I + H - TS + \Delta E_{\text{C-PCM}} - eU \tag{1}$$

Results

To gain deeper insights into the Cu-based DAC systems, we began our investigation with an analysis of their electronic structures. The π orbitals of the expanded porphyrins are highly delocalized, leading to HOMO-LUMO gaps that show consistent values across the series of DAC systems (Table S2, Figure S1). When adding an electron to simulate reduction, the CM5 partial atomic charges of the metal atoms undergoes negligible changes, suggesting the delocalization of the additional electron throughout the π system (Table S3). This observation implies that the CO_2 activation mechanism should predominately occur through a PCET mechanism, as the electron-deficient character of the DAC sites persists after an initial reduction. Notably, the π delocalization resulting from the additional electron does not induce stronger binding of CO_2 to either of the DAC sites.

In examining the hydrogen reduction performance of the EP-based DACs, we anticipate behavior akin to other porphyrin complexes, with an expected degree of ligand-centered activity.[45] Hydrogen adducts can form at several sites within the EP, encompassing metal atoms and porphyrinic nitrogen atoms. Figure 1 shows these adducts and their influence on

the planarity of the EP. Notably, nitrogen atoms forming hydrogen adducts must transition from trigonal planar (sp^2) to tetrahedral (sp^3) geometries, potentially affecting distinct porphyrin nitrogen atoms in a dissimilar manner. The energies of these adducts exhibit minor disparities, often differing by less than 0.22 eV (5.0 kcal mol^{-1}), indicating their likely formation under room temperature conditions. The limiting potentials for hydrogen reduction (Table S4, Figure 2) exhibit variation based on the secondary metal, with the CuZn and CuCo catalysts demonstrating the smallest values at 0.13 and 0.14 eV, respectively, while the CuMn and CuFe catalysts exhibit the largest values at 0.41 and 0.43 eV, respectively. The low limiting potential values observed for hydrogen reduction across the the six DACs suggest significant competition for the reduction of CO_2.

In the context of examining CO_2 reduction on the EP-based DACs, the reaction pathway reveals two distinct intermediates depending on whether the reaction proceeds at the C or O atom of the CO_2 molecule (Figure S2). Notably, the formation of the *OCHO intermediate consistently emerges as more energetically favorable than *OCOH across all DAC systems by a margin of 0.8-1.0 eV, and this preference is likely attributed to the creation of a bridging μ_2-OCHO species (top row of Figure 3). The *OCHO intermediate's structure remains relatively invariant when changing the secondary metal, suggesting that its favorable formation predominately stems from the geometry of the DAC and close proximity of the metal centers rather than the specific identity of the secondary metal. The intermetallic distance varies between 2.640 Å (CuMn) and 2.730 Å (CuCu) which is an optimal range for the favorable formation of μ_2 bridging intermediates (Table S5). This preference for the *OCHO intermediate entails a nearly complete hindrance in the formation of CO, which can only form from the *OCOH intermediate. Consequently, the expanded-porphyrin DAC complexes exhibit promising selectivity, particularly regarding the formation of the $2e^-$ product HCOOH.

A further reduction step shows that the formation of *HCOOH from the *OCHO intermediate is the most favorable across the DACs (Figure 3, second row from the top). While

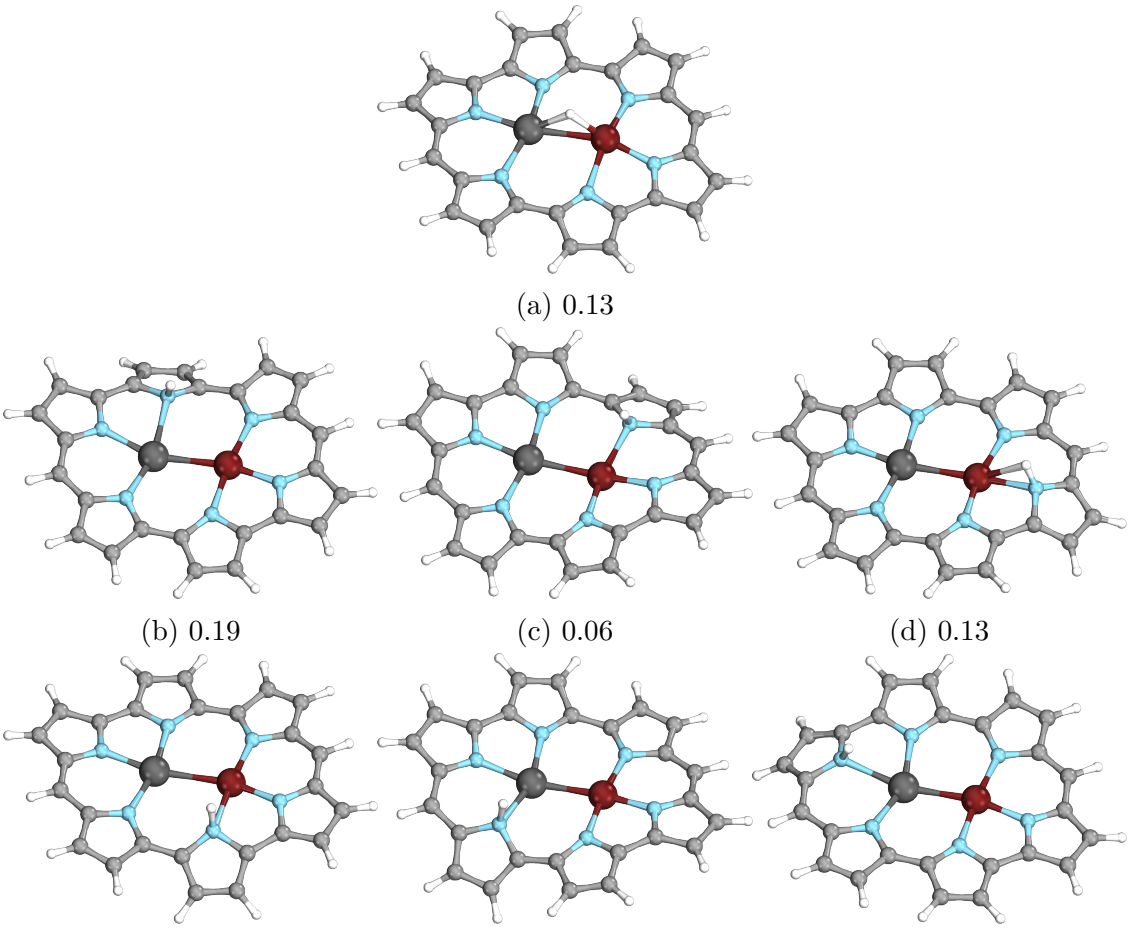

(a) 0.13

(b) 0.19 (c) 0.06 (d) 0.13

(e) 0.00 (f) 0.37 (g) 0.22

Figure 1: Hydrogen adducts on the CuMn EP. Values indicate relative free energies in eV. Color code: white - H, grey - C, blue - N, black - Mn, red - Cu.

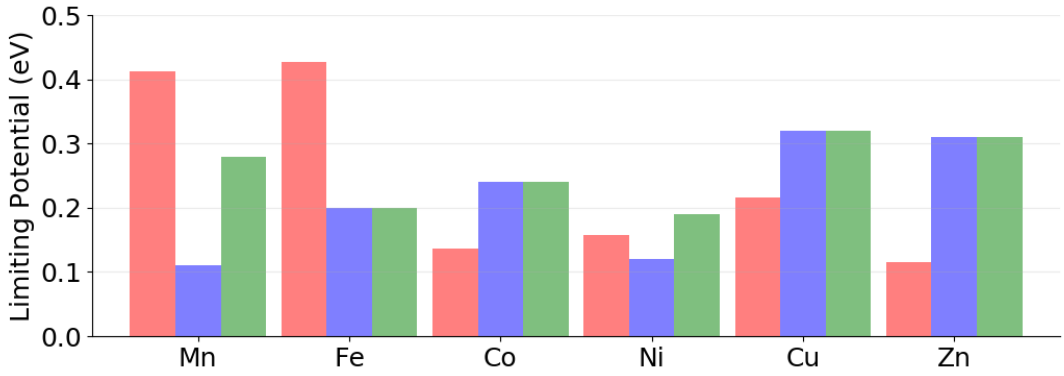

(a)

Figure 2: Limiting potentials for the H_2 (red), HCOOH, and H_2CO & H_2O (green) on the DACs.

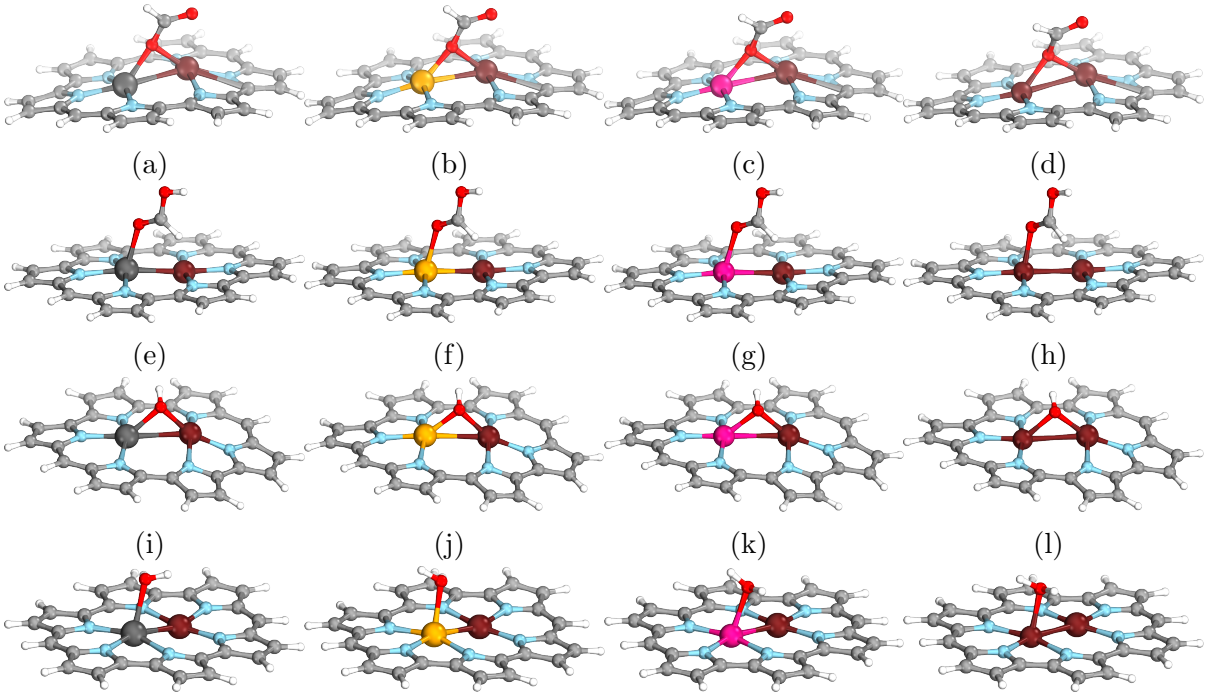

Figure 3: Rows from top-to-bottom depict the $^*OCHO$, $^*HCOOH$, $^*OH$, and $^*H_2O$ intermediates while columns from left-to-right depict the CuMn, CuFe, CuCo, and CuNi DACs. Color code: H - white, C - grey, O - red, brown - Cu.

alternative competitive pathways leading to $^*OCH_2O$ or $^*O$ (and H_2CO) intermediates exist, considerably higher formation energies (1.5-2.2 eV) render their formation on the DACs less probable. The process of forming $^*HCOOH$ requires overcoming a thermodynamic uphill barrier across all six DACs (Table 1), with energy inputs ranging from 0.02 eV (CuMn) to 0.31 eV (CuZn). The limiting potentials for H_2 (red) and HCOOH (blue) formation, depicted in Figure 2, offer valuable insights into the anticipated product selectivity on the DACs. CuCo, CuCu, and CuZn DACs favor the reduction of hydrogen to form H_2, while CO_2 reduction is more favorable on CuMn, CuFe, and CuNi DACs. Further reductions can occur with the $^*HCOOH$ intermediate given a strong enough interaction between the DAC surface.

The range of $^*HCOOH$ binding energies on the DACs spans 0.33 eV to -0.10 eV, where the former indicates unfavorable binding for HCOOH, while the latter suggests favorable binding. This behavior arises from shifts in the synergistic interaction between the two metal centers, with specific DAC configurations disrupting the scaling relationship and leading to disparate binding behaviors, as reported in recent literature.[46] CuMn and CuNi DACs exhibit favorable binding for the $^*HCOOH$ intermediate, suggesting that HCOOH will not constitute a large proportion of the products formed. Conversely, CuCu and CuZn DACs exhibit unfavorable HCOOH binding (0.33, and 0.16 eV, respectively), promoting the desorption of HCOOH rather than further reduction. This indicates that HCOOH and H_2 will be the predominant

Table 1: Reaction free energies for the reduction of CO_2 on the EP-based DACs. Values are relative to $^*CO_2$ and are given in eV.

	$^*OCHO$	$^*HCOOH$	$^*OH$ & H_2CO	$^*H_2O$
CuMn	0.11	0.13	0.41	0.24
CuFe	-0.05	0.15	0.20	0.26
CuCo	-0.11	0.13	0.20	0.19
CuNi	-0.01	0.11	0.30	0.15
CuCu	0.32	0.48	0.66	0.52
CuZn	-0.06	0.25	0.29	0.30

products for these two DACs. Lastly, CuFe and CuCo result in very weak binding (-0.005 eV), indicating a mixed product distribution due to both HCOOH desorption and further reduction occurring.

Following the formation of *HCOOH, four different intermediates can form following an additional PCET step: *HCO & H_2O, *HOCH$_2$O, *HOCHOH, or *OH & H_2CO. Notably, the formation of the *OH intermediate (Figure 3, second row from the bottom) is favored across all EP-based DACs, leading to the formation of H_2CO as a by-product. The PCET step most favorably attacks the C atom of *HCOOH which leads to the breaking of the C-O single bond and the subsequent formation of a μ_2-OH species. The favorable formation of the μ_2-OH species is akin to the μ_2-OCHO species discussed earlier, underscoring the EP-based DAC's ability to favor certain intermediates based on its geometry, irrespective of the secondary metal. The subsequent reduction step on the DACs leads to the formation of $^*H_2O$, marking the terminal stage of CO_2RR. Thus, the EP-based DACs are expected to produce only H_2, HCOOH, and H_2CO with varying selectivities.

Recognizing the inhibitory effect of the *OCHO intermediate on CO formation, we directed our focus towards assessing the potential of EP-based DACs to reduce CO in a manner akin to CO_2 reduction to see if more highly reduced products could be produced. We began first by determining the binding energy of CO across the six DACs, revealing a significant variation in contrast to the nearly identical CO_2 binding behavior observed earlier (see Table S6). Specifically, CuNi exhibited a strong affinity for CO at -0.38 eV, while CuMn demonstrated relatively weak binding at -0.04 eV. CuFe, CuCo, and CuZn showcased marginally unfavorable binding of CO within a range of 0.05 to 0.08 eV, whereas CuCu displayed a pronounced disfavor towards CO binding by 0.84 eV. These findings highlight the influence of the secondary metal on the CO reduction process, emphasizing the need for a heteronuclear DAC complex in fostering favorable CO binding. Evidently, the weak CO binding on all DACs except CuNi suggest the potential viability of CO reduction exclusively on the

CuNi surface, while the remaining DACs may display limited CO reduction activity. Thus, we proceeded to undertake a more comprehensive exploration of CO reduction specifically focused on the CuNi DAC.

The initial step in the reduction of CO offers two distinct pathways: reduction at the C or the O atom, yielding the *HCO or *COH intermediates, respectively (Figure S3). *HCO emerges as more energetically favorable; however, the formation process is endergonic, requiring an input of 0.80 eV to proceed. Subsequent steps, as shown in Figure S3, proceed in an exergonic fashion. Starting with *HCO, the reaction leads to the formation of $^*H_2CO$ followed by $^*CH_3O$, $^*CH_3OH$, *OH (& CH_4), and finally $^*H_2O$. The short intermetallic distance between the Cu and Ni centers (2.715 Å) facilitates the emergence of μ_2 bridging geometries for *CO, *HCO, $^*CH_3O$, and *OH intermediates. The reduced CO intermediates are adsorbed strongly to the surface of the CuNi DAC, thus enabling their complete reduction to CH_4 and H_2O. The limiting potential is calculated to be 0.80 eV which far surpasses that of hydrogen reduction on the CuNi DAC. This disparity suggests significant competition between the reduction of CO and hydrogen, rendering CO reduction significantly less favorable. Comparable limiting potentials were observed across the DACs, ranging from 0.56 eV (CuCo) to 0.95 eV (CuZn), indicating their likewise strong likelihood of being out-competed by HER. Consequently, while the prospect of CO reduction remains feasible using the EP-based DACs, the thermodynamic favorability leans distinctly towards hydrogen and CO_2 reduction pathways.

Discussion

Both the reduction of hydrogen and CO_2 are expected to proceed on the EP-based DACs with low limiting potentials of less than 0.43 and 0.32 eV, respectively, while the reduction of CO is expected to not proceed favorably on any of the EP-based DACs. Figure 4 shows

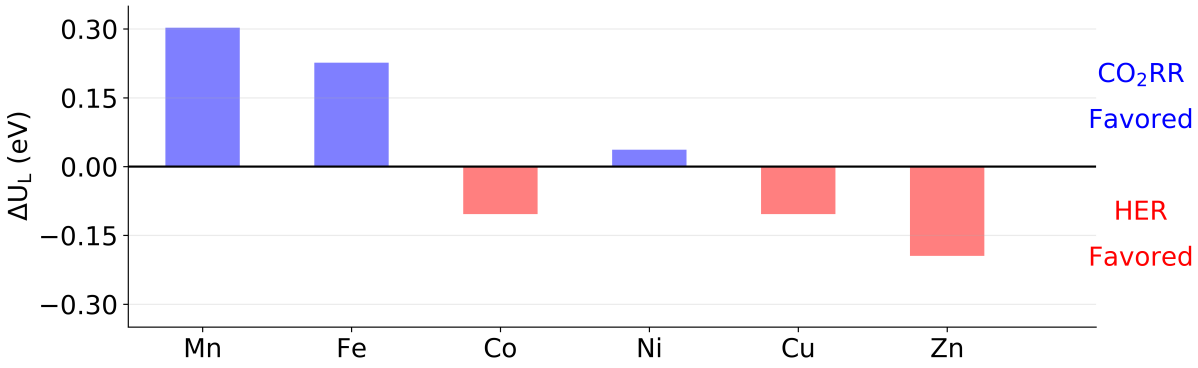

Figure 4: Difference in HCOOH and H_2 limiting potentials on the DACs. Blue bars indicate that CO_2RR is more favored while red bars indicate that HER is more favored.

the differences between the limiting potentials for H_2 and HCOOH, which allows for an estimation of the selectivity between HER and CO_2RR. CuMn and CuFe reduce CO_2 more favorably than hydrogen, as evidenced in the blue bars in Figure 4, while CuCo, CuCu, and CuZn more favorably reduce hydrogen. Thus, a selectivity difference should be observed among these DACs in which more reduced CO_2 products are produced using CuMn and CuFe and more H_2 is produced using CuCo, CuCu, and CuZn. CuNi is expected to produce similar amounts of H_2 and reduced CO_2 products due to the small difference between the limiting potentials.

As mentioned previously, the *HCOOH intermediate is not favorably bound to the surface of the CuCu or CuZn DACs, thus selectively leading to the formation of only HCOOH. Conversely, the CuMn and CuNi DACs exhibit strong binding of *HCOOH, which is expected to push the reaction to produce more highly reduced products, namely H_2CO. The formation of the *OH intermediate during the third reduction step of the reaction yields H_2CO as a by-product which is less strongly bound to the surface of the CuMn and CuNi DACs, thus leading to the selective formation of H_2CO and H_2O. The CuMn and CuNi DACs also exhibit different limiting potentials for HCOOH and H_2CO formation, suggesting that higher potentials must be utilized in order to make the formation of H_2CO favorable. The

two remaining DACs, CuFe and CuCo, are expected to reduce CO_2 to both HCOOH and H_2CO due to the weak but favorable binding of *HCOOH. Based on the limiting potentials for H_2, HCOOH, and H_2CO, different product distributions are expected for the six DACs: CuMn and CuFe are expected to selectively produce reduced CO_2 products with CuMn favoring the formation of H_2CO and CuFe favoring both HCOOH and H_2CO, CuCo, CuCu, and CuZn are expected to predominately produce H_2 with some reduced CO_2 intermediates, and CuNi is expected to produce similar amounts of both H_2 and H_2CO with little formation of HCOOH.

The unique ligand environment provided by the expanded porphyrin places two metal centers in close proximity to one another, which is pivotal for the discussed reduction processes. This environment can be further tailored through heteroatom doping within the ligand structure or by employing diverse combinations of metal centers to fine-tune the reduction mechanisms. Furthermore, the ligand framework can be integrated into heterogeneous structures like metal-organic frameworks to explore analogous or diverse realms of chemistry. While numerous porphyrin-based MOFs have been successfully synthesized and investigated,[47] it's noteworthy that we could not identify any MOFs incorporating EP-based ligand scaffolds. This discovery highlights an as-yet-unexplored frontier in the domains of both chemistry and materials science.

Conclusions

Six DACs were examined using DFT to understand the secondary metal effects on the reduction of hydrogen, CO_2, and CO. Our model system involved a simplified expanded porphyrin ligand scaffold in which one of the Cu sites was replaced with another transition metal (Mn, Fe, Co, Ni, Cu, or Zn). Slight variations were observed for the reduction of hydrogen on the six DACs and the process is expected to proceed with limiting potentials

between 0.13 eV (CuCu, CuZn) and 0.43 eV (CuMn, CuFe). The DACs that involve later transition metals are expected to favor the reduction of hydrogen to form H_2 due to the very small limiting potentials. The reduction of CO_2 is expected to produce only $2e^-$ and $4e^-$ reduced CO_2 products: HCOOH and H_2CO, respectively. The favorability of two specific intermediates precludes the formation of any other reduced CO_2 products with *OCHO limiting the probability of CO formation while *OH signifies the end of the reduction process with the formation of H_2CO. CuMn and CuFe DACs are expected to favorably produce more reduced CO_2 products while CuCo, CuCu, and CuZn are expected to favor the formation of H_2. Lastly, CO reduction was examined on the CuNi DAC but the process was found to occur with a limiting potential of 0.80 eV which is significantly higher than that for hydrogen reduction, thus limiting the feasibility of CO reduction on the CuNi DAC.

Acknowledgement

G.A.M would like to thank NIST's Postdoctoral Program for an NRC Postdoctoral Fellowship.

Supporting Information Available

The supporting information (Supporting Information.pdf) contains additional information which helps support the research presented in this manuscript. Additionally, the files "Supporting Information - Energy.xlsx" and "Coordinates.zip" contain the energetic information and Cartesian coordinates for every structure used for this work, respectively.

References

(1) Jones, M. W.; Peters, G. P.; Gasser, T.; Andrew, R. M.; Schwingshackl, C.; Gütschow, J.; Houghton, R. A.; Friedlingstein, P.; Pongratz, J.; Le Quéré, C. National contributions to climate change due to historical emissions of carbon dioxide, methane, and nitrous oxide since 1850. *Scientific Data* **2023**, *10*, 155.

(2) Vitillo, J. G.; Smit, B.; Gagliardi, L. Introduction: Carbon Capture and Separation. *Chemical Reviews* **2017**, *117*, 9521–9523.

(3) van de Ven, D.-J. et al. A multimodel analysis of post-Glasgow climate targets and feasibility challenges. *Nature Climate Change* **2023**, *13*, 570–578.

(4) Sanz-Pérez, E. S.; Murdock, C. R.; Didas, S. A.; Jones, C. W. Direct Capture of CO_2 from Ambient Air. *Chemical Reviews* **2016**, *116*, 11840–11876.

(5) Gao, W. et al. Industrial carbon dioxide capture and utilization: state of the art and future challenges. *Chemical Society Reviews* **2020**, *49*, 8584–8686.

(6) Yousaf, M.; Zaman, M.; Mahmood, A.; Imran, M.; Elkamel, A.; Rizwan, M.; Wilberforce, T.; Riaz, F. Carbon dioxide utilization: A critical review from multiscale perspective. *Energy Science & Engineering* **2022**, *10*, 4890–4923.

(7) Ali, M.; Jha, N. K.; Pal, N.; Keshavarz, A.; Hoteit, H.; Sarmadivaleh, M. Recent advances in carbon dioxide geological storage, experimental procedures, influencing parameters, and future outlook. *Earth-Science Reviews* **2022**, *225*, 103895.

(8) Francke, R.; Schille, B.; Roemelt, M. Homogeneously Catalyzed Electroreduction of Carbon Dioxide—Methods, Mechanisms, and Catalysts. *Chemical Reviews* **2018**, *118*, 4631–4701.

(9) Jiang, X.; Nie, X.; Guo, X.; Song, C.; Chen, J. G. Recent Advances in Carbon Dioxide Hydrogenation to Methanol via Heterogeneous Catalysis. *Chemical Reviews* **2020**, *120*, 7984–8034.

(10) Cui, L.; Liu, C.; Yao, B.; Edwards, P. P.; Xiao, T.; Cao, F. A review of catalytic hydrogenation of carbon dioxide: From waste to hydrocarbons. *Frontiers in Chemistry* **2022**, *10*.

(11) Li, W.; Wang, H.; Jiang, X.; Zhu, J.; Liu, Z.; Guo, X.; Song, C. A short review of recent advances in CO_2 hydrogenation to hydrocarbons over heterogeneous catalysts. *RSC Advances* **2018**, *8*, 7651–7669.

(12) Kumaravel, V.; Bartlett, J.; Pillai, S. C. Photoelectrochemical Conversion of Carbon Dioxide (CO_2) into Fuels and Value-Added Products. *ACS Energy Letters* **2020**, *5*, 486–519.

(13) Nitopi, S.; Bertheussen, E.; Scott, S. B.; Liu, X.; Engstfeld, A. K.; Horch, S.; Seger, B.; Stephens, I. E. L.; Chan, K.; Hahn, C.; Nørskov, J. K.; Jaramillo, T. F.; Chorkendorff, I. Progress and Perspectives of Electrochemical CO_2 Reduction on Copper in Aqueous Electrolyte. *Chemical Reviews* **2019**, *119*, 7610–7672.

(14) Song, W.; Xiao, C.; Ding, J.; Huang, Z.; Yang, X.; Zhang, T.; Mitlin, D.; Hu, W. Review of Carbon Support Coordination Environments for Single Metal Atom Electrocatalysts (SACS). *Advanced Materials* **2023**,

(15) Wang, T.; Zhang, J.; Li, F.; Liu, B.; Kawi, S. Recent progress of electrochemical reduction of CO_2 by single atom catalysts. *Materials Reports: Energy* **2022**, *2*, 100140.

(16) McCarver, G. A.; Yildirim, T.; Zhou, W. Computational Examination of Transition Metal-Salen Complexes for the Reduction of CO_2. *Under Review*

(17) Abdinejad, M.; Yuan, T.; Tang, K.; Duangdangchote, S.; Farzi, A.; Iglesias van Montfort, H.; Li, M.; Middelkoop, J.; Wolff, M.; Seifitokaldani, A.; Voznyy, O.; Burdyny, T. Electroreduction of Carbon Dioxide to Acetate using Heterogenized Hydrophilic Manganese Porphyrins. *Chemistry – A European Journal* **2023**, *29*.

(18) Call, A.; Cibian, M.; Yamamoto, K.; Nakazono, T.; Yamauchi, K.; Sakai, K. Highly Efficient and Selective Photocatalytic CO_2 Reduction to CO in Water by a Cobalt Porphyrin Molecular Catalyst. *ACS Catalysis* **2019**, *9*, 4867–4874.

(19) Pu, T.; Ding, J.; Zhang, F.; Wang, K.; Cao, N.; Hensen, E. J. M.; Xie, P. Dual Atom Catalysts for Energy and Environmental Applications. *Angewandte Chemie International Edition* **2023**,

(20) Yu, L.; Li, F.; Huang, J.; Sumpter, B. G.; Mustain, W. E.; Chen, Z. Double-Atom Catalysts Featuring Inverse Sandwich Structure for CO_2 Reduction Reaction: A Synergetic First-Principles and Machine Learning Investigation. *ACS Catalysis* **2023**, *13*, 9616–9628.

(21) Yang, W.; Jia, Z.; Zhou, B.; Chen, L.; Ding, X.; Jiao, L.; Zheng, H.; Gao, Z.; Wang, Q.; Li, H. Why Is C–C Coupling in CO_2 Reduction Still Difficult on Dual-Atom Electrocatalysts? *ACS Catalysis* **2023**, *13*, 9695–9705.

(22) Bai, Z.; Jiang, X. Z.; Luo, K. H. Theoretical exploration on the performance of single and dual-atom Cu catalysts on the CO_2 electroreduction process: A DFT study. *Physical Chemistry Chemical Physics* **2023**,

(23) Yang, W.; Jia, Z.; Chen, L.; Zhou, B.; Zhang, D.; Han, Y.; Gao, Z.; Li, H. Effects of intermetal distance on the electrochemistry-induced surface coverage of M–N–C dual-atom catalysts. *Chemical Communications* **2023**, *59*, 10761–10764.

(24) Ding, J.; Li, F.; Zhang, J.; Zhang, Q.; Liu, Y.; Wang, W.; Liu, W.; Wang, B.; Cai, J.; Su, X.; Yang, H. B.; Yang, X.; Huang, Y.; Zhai, Y.; Liu, B. Circumventing CO_2 Reduction Scaling Relations Over the Heteronuclear Diatomic Catalytic Pair. *Journal of the American Chemical Society* **2023**, *21*, 11829–11836.

(25) Qiu, X.-F.; Zhu, H.-L.; Huang, J.-R.; Liao, P.-Q.; Chen, X.-M. Highly Selective CO_2 Electroreduction to C_2H_4 Using a Metal–Organic Framework with Dual Active Sites. *Journal of the American Chemical Society* **2021**, *143*, 7242–7246.

(26) Weghorn, S. J.; Sessler, J. L.; Lynch, V.; Baumann, T. F.; Sibert, J. W. Bis[(μ-chloro)copper(II)] Amethyrin: A Bimetallic Copper(II) Complex of an Expanded Porphyrin. *Inorganic Chemistry* **1996**, *35*, 1089–1090.

(27) Jiang, J.; Materna, K. L.; Hedström, S.; Yang, K. R.; Crabtree, R. H.; Batista, V. S.; Brudvig, G. W. Antimony Complexes for Electrocatalysis: Activity of a Main-Group Element in Proton Reduction. *Angewandte Chemie International Edition* **2017**, *56*, 9111–9115.

(28) Xiao, W.-C.; Tao, Y.-W.; Luo, G.-G. Hydrogen formation using a synthetic heavier main-group bismuth-based electrocatalyst. *International Journal of Hydrogen Energy* **2020**, *45*, 8177–8185.

(29) Williams, C. K.; McCarver, G. A.; Lashgari, A.; Vogiatzis, K. D.; Jiang, J. . *Inorganic Chemistry* **2021**, *60*, 4915–4923.

(30) Williams, C.; McCarver, G.; Chaturvedi, A.; Sinha, S.; Ang, M.; Vogiatzis, K.; Jiang, J. Electrocatalytic Hydrogen Evolution Using A Molecular Antimony Complex under Aqueous Conditions: An Experimental and Computational Study on Main-Group Element Catalysis. *Chemistry - A European Journal* **2022**, *28*.

(31) Chaturvedi, A.; McCarver, G.; Sinha, S.; Hix, E.; Vogiatzis, K.; Jiang, J. A PEGylated Tin Porphyrin Complex for Electrocatalytic Proton Reduction: Mechanistic Insights into Main-Group-Element Catalysis. *Angewandte Chemie - International Edition* **2022**,

(32) Slater, J. C.; Johnson, K. H. Self-Consistent-Field Xα Cluster Method for Polyatomic Molecules and Solids. *Physical Review B* **1972**, *5*, 844–853.

(33) Lee, C.; Yang, W.; Parr, R. G. Development of the Colle-Salvetti correlation-energy formula into a functional of the electron density. *Physical Review B* **1988**, *37*, 785–789.

(34) Neese, F.; Wennmohs, F.; Becker, U.; Riplinger, C. The ORCA quantum chemistry program package. *The Journal of Chemical Physics* **2020**, *152*, 224108.

(35) Grimme, S.; Antony, J.; Ehrlich, S.; Krieg, H. A consistent and accurate *ab initio* parametrization of density functional dispersion correction (DFT-D) for the 94 elements H-Pu. *The Journal of Chemical Physics* **2010**, *132*, 154104.

(36) Johnson, E. R.; Becke, A. D. A post-Hartree-Fock model of intermolecular interactions: Inclusion of higher-order corrections. *The Journal of Chemical Physics* **2006**, *124*, 174104.

(37) Kalinowski, J.; Wennmohs, F.; Neese, F. Arbitrary Angular Momentum Electron Repulsion Integrals with Graphical Processing Units: Application to the Resolution of Identity Hartree–Fock Method. *Journal of Chemical Theory and Computation* **2017**, *13*, 3160–3170.

(38) Weigend, F. Accurate Coulomb-fitting basis sets for H to Rn. *Physical Chemistry Chemical Physics* **2006**, *8*, 1057.

(39) Barone, V.; Cossi, M. Quantum Calculation of Molecular Energies and Energy Gradi-

ents in Solution by a Conductor Solvent Model. *The Journal of Physical Chemistry A* **1998**, *102*, 1995–2001.

(40) Marenich, A. V.; Jerome, S. V.; Cramer, C. J.; Truhlar, D. G. Charge Model 5: An Extension of Hirshfeld Population Analysis for the Accurate Description of Molecular Interactions in Gaseous and Condensed Phases. *Journal of Chemical Theory and Computation* **2012**, *8*, 527–541.

(41) Lu, T.; Chen, F. Multiwfn: A multifunctional wavefunction analyzer. *Journal of Computational Chemistry* **2012**, *33*, 580–592.

(42) Weinberg, D. R.; Gagliardi, C. J.; Hull, J. F.; Murphy, C. F.; Kent, C. A.; Westlake, B. C.; Paul, A.; Ess, D. H.; McCafferty, D. G.; Meyer, T. J. Proton-Coupled Electron Transfer. *Chemical Reviews* **2012**, *112*, 4016–4093.

(43) Tyburski, R.; Liu, T.; Glover, S. D.; Hammarström, L. Proton-Coupled Electron Transfer Guidelines, Fair and Square. *Journal of the American Chemical Society* **2021**, *143*, 560–576.

(44) Peterson, A. A.; Abild-Pedersen, F.; Studt, F.; Rossmeisl, J.; Nørskov, J. K. How copper catalyzes the electroreduction of carbon dioxide into hydrocarbon fuels. *Energy and Environmental Science* **2010**, *3*.

(45) Castro-Cruz, H. M.; Macías-Ruvalcaba, N. A. Porphyrin-catalyzed electrochemical hydrogen evolution reaction. Metal-centered and ligand-centered mechanisms. *Coordination Chemistry Reviews* **2022**, *458*, 214430.

(46) Tang, T.; Wang, Z.; Guan, J. Structural optimization of carbon-based diatomic catalysts towards advanced electrocatalysis. *Coordination Chemistry Reviews* **2023**, *492*, 215288.

(47) Zhang, X. et al. A historical perspective on porphyrin-based metal–organic frameworks and their applications. *Coordination Chemistry Reviews* **2021**, *429*, 213615.

TOC Graphic